

Phases of the (2+1) dimensional SO(5) non-linear sigma model with topological term

Zhenjiu Wang,^{1,*} Michael P. Zaletel,² Roger S. K. Mong,³ and Fakhre F. Assaad^{1,4,†}

¹*Institut für Theoretische Physik und Astrophysik,
Universität Würzburg, 97074 Würzburg, Germany*

²*Department of Physics, University of California, Berkeley, CA 94720, USA*

³*Department of Physics and Astronomy, University of Pittsburgh, Pittsburgh, PA 15260, USA*

⁴*Würzburg-Dresden Cluster of Excellence ct.qmat, Am Hubland, D-97074 Würzburg, Germany*

We use the half-filled zeroth Landau level in graphene as a regularization scheme to study the physics of the SO(5) non-linear sigma model subject to a Wess-Zumino-Witten topological term in 2+1 dimensions. As shown by Ippoliti et al. [PRB 98, 235108 (2019)], this approach allows for negative sign free auxiliary field quantum Monte Carlo simulations. The model has a single free parameter, U_0 , that monitors the stiffness. Within the parameter range accessible to negative sign free simulations, we observe an ordered phase in the large U_0 or stiff limit. Remarkably, upon reducing U_0 the magnetization drops substantially, and the correlation length exceeds our biggest system sizes, accommodating 100 flux quanta. The implications of our results for deconfined quantum phase transitions between valence bond solids and anti-ferromagnets are discussed.

Introduction. At critical points the renormalization group allows for the definition of emergent symmetries and field theories. For example, the semi-metal to insulator transitions in graphene^{1–3} have an emergent Lorentz symmetry^{4,5} so that space and time can interchangeably be used⁶ to efficiently compute critical exponents. Models that capture the physics of deconfined quantum criticality (DQC)^{7,8} – the JQ model for example⁹ – have an $SO(3) \times C_4$ symmetry, but at criticality the C_4 point group is enlarged to a higher $U(1)$ symmetry. Improved models, with $SO(3) \times U(1)$ symmetry have been proposed to study DQC.¹⁰ Formulating the theory of DQC with eight component Dirac fermions akin to graphene and Yukawa coupled to a quintuplet of anti-commuting mass terms¹¹ quite naturally leads to the conjecture of an emergent SO(5) symmetry.^{12–14} Compelling numerical evidence for this emergent symmetry has been put forward¹⁵ in the realm of loop models.¹⁶

Let us now consider a phase transition with enhanced symmetry and a relevant operator α which breaks it. In this case, formulating a model with higher symmetry allows us to assess the nature of the transition. Schematic RG flows for an enhanced SO(5) symmetry that is broken down to $SO(3) \times SO(2)$ are shown in Fig. 1. While α breaks the SO(5) symmetry, U_0 conserves it. If the higher symmetry model is in an ordered phase, then the transition is first order [Fig. 1(a)]. The spin-flop transition corresponding to the field-driven reorientation of the easy axis falls into this category. Alternatively, the enhanced symmetry model can be critical such that the transition is continuous [Fig. 1(b)]. As an example for this scenario, we can consider the one-dimensional DQC between a dimer and Néel state in the XXZ model considered in Refs.^{17,18} and realized in.¹⁹ The critical point has

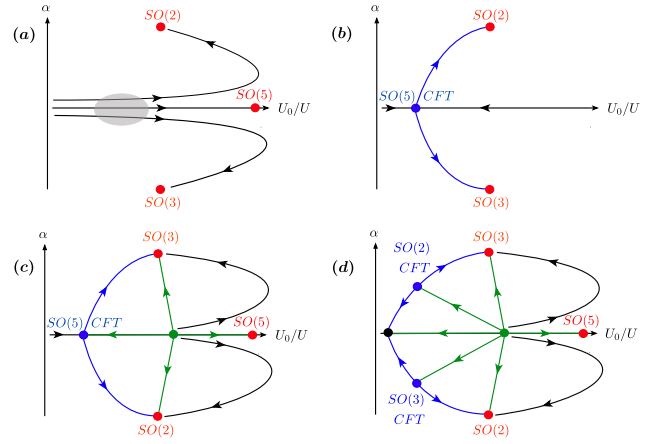


FIG. 1. Possible RG flows in the U_0 versus α phase. α corresponds to the amplitude of a term that breaks down the SO(5) symmetry to $SO(3) \times SO(2)$. The horizontal line corresponds to the $\alpha = 0$ or to SO(5) symmetry. Red bullets, corresponds to phases where the symmetry group is spontaneously broken. The black bullet is an SO(5) disordered phase. Blue (green) bullets denote critical (multi-critical) points. In scenario (a) the SO(5) model orders and the shaded region depicts a slow RG flow (see text). In (b) the SO(5) model remains critical. In (c) the SO(5) model has an ordered and critical phase separated by a multi-critical point. Finally, in (d) the SO(5) model shows an order-disorder transition.

a $U(1)$ symmetry that is broken by the umklapp operator that tunes through the transition. As a third possibility, the enhanced-symmetry model may have a relevant tuning parameter U_0 – and associated (multi) critical point – that does not break the enhanced symmetry. Fig. 1(c) describes a scenario where the ordered state gives way to a critical phase. In this case, tuning α leads to first order or continuous transitions depending upon the value of U_0 . Finally, in Fig. 1(d) U_0 drives an order-disorder transition. Aside from fine tuning, the transition from the SO(3) to SO(2) broken symmetry states is first order

* Zhenjiu.Wang@physik.uni-wuerzburg.de

† assaad@physik.uni-wuerzburg.de

or separated by a disordered phase.

The aim of this letter is to investigate the $O(5)$ nonlinear sigma model in 2+1 dimensions with a Wess-Zumino-Witten geometrical term. As mentioned above, this model can be obtained by integrating out quintuplets of anti-commuting mass terms in Dirac systems.¹²⁻¹⁴

$$S = \frac{1}{g} \int d^3x (\nabla \hat{\varphi})^2 + S_{\text{WZW}}. \quad (1)$$

Here $\hat{\varphi}$ corresponds to a five-dimensional unit vector. The model has a manifest $SO(5)$ symmetry, and a single parameter, the stiffness. The question we would like to address in this work is the nature of the phase diagram as a function of the stiffness.

Model and method. The work of Ippoliti et al.²⁰ demonstrates that a nonlinear sigma model with exact $SO(5)$ symmetry can be constructed using 8 component Dirac fermions quenched in the zeroth Dirac Landau level (ZLL). As opposed to a lattice approach, one remains in continuum space time, but the single particle Hilbert space remains finite and counts the $4N_\phi$ states of the ZLL, where N_ϕ is the number of magnetic fluxes piercing the two dimensional space. The model reads:

$$\hat{H} = \int_V d^2\mathbf{x} \left(\frac{U_0}{2} [\hat{\psi}^\dagger(\mathbf{x})\hat{\psi}(\mathbf{x}) - C(\mathbf{x})]^2 - \frac{U}{2} \sum_{i=1}^5 [\hat{\psi}^\dagger(\mathbf{x}) O^i \hat{\psi}(\mathbf{x})]^2 \right) \quad (2)$$

where the fermion annihilation operator are projected onto the ZLL: $\hat{\psi}_a(\mathbf{x}) = \sum_{k=1}^{N_\phi} \phi_k(\mathbf{x}) \hat{c}_{a,k}$. The index a runs from $1 \cdots 4$ corresponding to the four Dirac ZLLs. It's crucial that the operators $\hat{\psi}(\mathbf{x})$ ($\hat{\psi}^\dagger(\mathbf{x})$) do not satisfy the canonical commutation rules due to the projection. The wave functions of the ZLL, $\phi_{k_y}(\mathbf{x})$, are computed in the Landau gauge which diagonalizes the translation invariance along one direction (see SM). The background $C(\mathbf{x}) \equiv 2 \sum_{k_y=1}^{N_\phi} |\phi_{k_y}(\mathbf{x})|^2$ ensures particle-hole symmetry in Eq. (2).

For $i = 1 \cdots 5$, O^i , are mutually anti-commuting matrices. A convenient choice reads:

$$\tau_x \otimes \mathbb{1}_2, \tau_y \otimes \mathbb{1}_2, \tau_z \otimes \vec{\tau} \quad i = 1, 2, \dots, 5. \quad (3)$$

The 10 matrices $L^{ij} = -\frac{i}{2} [O^i, O^j]$, $i, j = 1 \cdots 5$, are the generators of the $SO(5)$ group and commute with the Hamiltonian. Along the $SO(5)$ high symmetry line, the Hamiltonian has only one energy scale U_0/U .

Let $\varphi_i(\mathbf{x}) = \langle \hat{\psi}^\dagger(\mathbf{x}) O^i \hat{\psi}(\mathbf{x}) \rangle$ and assume that the mass gap $\Delta \propto |\varphi|$ is finite. One can then omit amplitude fluctuations of the vector $\varphi(\mathbf{x})$, integrate of the fermions in the large mass approximation to obtain an effective field theory for $\hat{\varphi}(\mathbf{x}) \equiv \varphi(\mathbf{x})/|\varphi(\mathbf{x})|$ that corresponds precisely to Eq. (1).²¹ Here, we identify U_0/U to $1/g$.

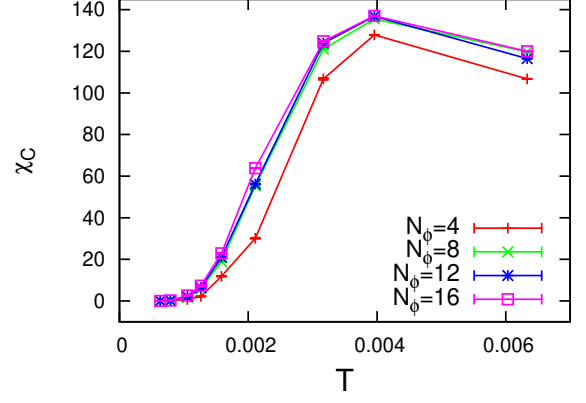


FIG. 2. Temperature dependence of the uniform charge susceptibility χ_C for $U_0 = -1$.

As mentioned previously, our numerical simulations are based on the work of Ippoliti et al.²⁰ that show how to formulate a negative sign free auxiliary field QMC for the Hamiltonian of Eq. (2) in the parameter range $U_0/U \geq -1$. The algorithm is formulated in Fourier space,

$$\hat{H} = \frac{1}{2V} \sum_{\mathbf{q}} \left(U_0 \hat{n}(\mathbf{q}) \hat{n}(-\mathbf{q}) - U \sum_{i=1}^5 \hat{n}^i(\mathbf{q}) \hat{n}^i(-\mathbf{q}) \right), \quad (4)$$

with $\hat{\psi}^\dagger(\mathbf{x}) O^i \hat{\psi}(\mathbf{x}) = \frac{1}{V} \sum_{\mathbf{q}} e^{-i\mathbf{q} \cdot \mathbf{x}} \hat{n}^i(\mathbf{q})$ and $\hat{\psi}^\dagger(\mathbf{x}) \hat{\psi}(\mathbf{x}) - C(\mathbf{x}) = \frac{1}{V} \sum_{\mathbf{q}} e^{-i\mathbf{q} \cdot \mathbf{x}} \hat{n}(\mathbf{q})$. As shown in the supplemental material (SM) one key point is to use a Fierz identity to avoid the negative sign problem. For each \mathbf{q} we then use a complex Hubbard-Stratonovich transformation to decouple the interaction term. Auxiliary field QMC simulations turn out to be involved. The difficulty lies in the fact that the projected density operators are not local and that they do not commute with each other. In the SM we show that for a symmetric Trotter decomposition, that preserves the hermiticity of the imaginary time propagation, the systematic error scales as $(\Delta\tau N_\phi)^2$. Here we have set the magnetic unit length, l_B , to unity such that N_ϕ corresponds to the volume. We also note that the $SO(5)$ symmetry is broken by the Trotter decomposition such that it potentially introduces a relevant operator. For all these reasons, great care has to be taken to control the systematic error, and we are obliged to scale $\Delta\tau$ as $1/N_\phi$. A detailed account of the Trotter error is given in the SM. Since we are working in the continuum, the sum over momenta is not bounded. However, the density operator contains a factor $e^{-\frac{1}{4}\mathbf{q}^2 l_B^2}$ and momenta that exceed a critical value can be safely omitted. Adopting this regularization strategy restricts the sum over momenta to order N_ϕ values again for the case $l_B = 1$. Again a detailed test of the choice of the momenta cutoff

is given in the supplemental material. Taking all the above into account yields a computational effort that scales as $N_\phi^5 \beta$ where β is the inverse temperature. This should be compared to the generic $N_\phi^3 \beta$ scaling for say the Hubbard model. The above explains why our simulations are limited to $N_\phi = 100$. We have used the finite temperature auxiliary field algorithm^{22–24} of the algorithms for lattice fermions (ALF)-library.²⁵ The details of our implementation are discussed in the SM.

Numerical results. For the simulations we set the energy scale by choosing $U = 1$, the length scale by choosing $l_B = 1$ and vary U_0 and the volume N_ϕ . We found that an inverse temperature of $\beta = 160\pi^2$ suffices to obtain ground state properties on our largest system sizes, $N_\phi = 100$.

In Fig. 2 we plot the uniform charge susceptibility,

$$\chi_C = \frac{\beta}{N_\phi} (\langle \hat{n}_{\mathbf{q}=0} \hat{n}_{\mathbf{q}=0} \rangle - \langle \hat{n}_{\mathbf{q}=0} \rangle \langle \hat{n}_{\mathbf{q}=0} \rangle). \quad (5)$$

The charge fluctuations decay exponentially upon reducing the temperature as expected for an insulating state of matter. Since $\hat{\psi}^\dagger(\mathbf{x}) O^i \hat{\psi}(\mathbf{x})$ are mass terms, any non-vanishing expectation value of these fermion bilinears, φ_i , will lead to a charge gap. Owing to the SO(5) symmetry the single particle gap is proportional to the norm of this five component vector, $|\varphi|$.

Although $|\varphi|$ is finite, phase fluctuations can destroy ordering. To numerically investigate this possibility, we compute the order parameter correlation function

$$S(\mathbf{q}) = \frac{1}{N_\phi} \sum_{i=1}^5 \langle \hat{n}_{\mathbf{q}}^i \hat{n}_{-\mathbf{q}}^i \rangle. \quad (6)$$

For an ordering wave vector \mathbf{Q} , the local moment reads

$$m = \sqrt{\frac{1}{N_\phi} S(\mathbf{Q})} \quad (7)$$

and it is convenient to define a renormalization group invariant quantity

$$R \equiv 1 - \frac{S(\mathbf{Q} + \Delta\mathbf{q})}{S(\mathbf{Q})} \quad (8)$$

with $|\Delta\mathbf{q}| = \frac{2\pi}{\sqrt{N_\phi}}$. In the ordered (disordered) phase R converges to unity (zero) and the local moment takes a finite (vanishing) value. At a critical point, the correlation ratio converges to a universal value.

In Fig. 3(a) we plot the correlation ratio R as a function of system size for various values of U_0 . For system sizes up to $N_\phi = 20$ all curves scale downwards and would suggest a critical or disordered phase. Beyond $N_\phi = 20$ and for large values of U_0 the correlation ratio changes behavior and grows. The length scale at which this crossover occurs can naturally be interpreted as a measure of the

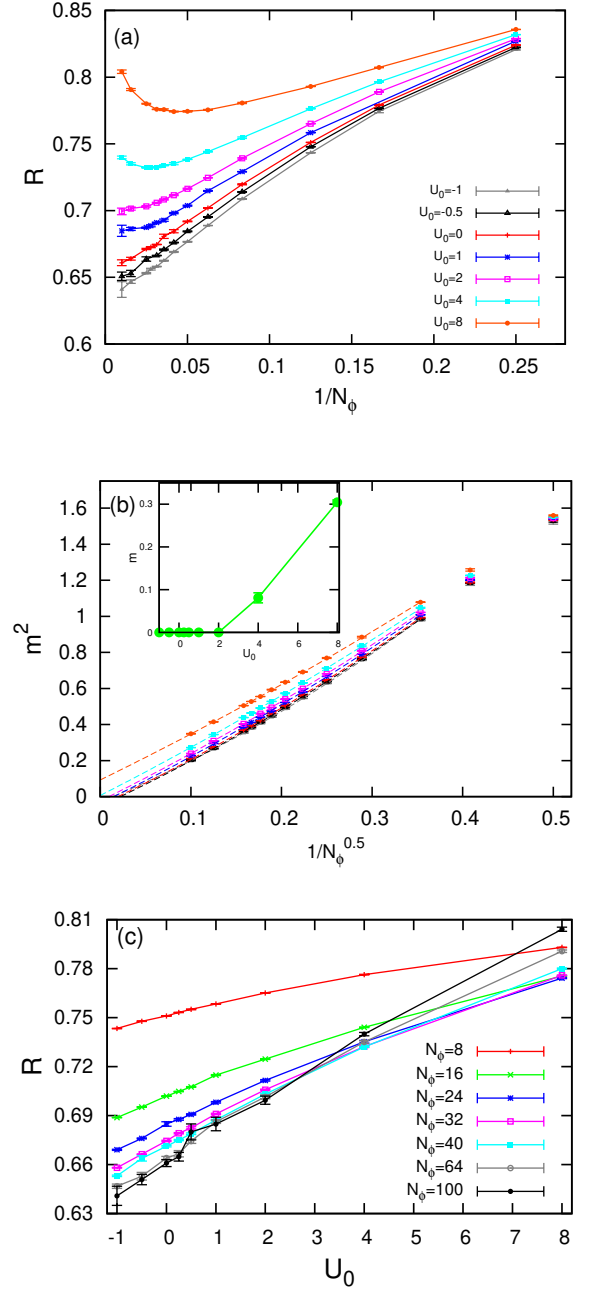


FIG. 3. Correlation ratio R as a function of $1/N_\phi$ (a) and U_0 (c), as well as the O(5) order parameter (b) as a function of $1/\sqrt{N_\phi}$. The dashed lines and the inset is the extrapolation via the fitting form $m(N_\phi)^2 = m_{N_\phi \rightarrow \infty}^2 + a/\sqrt{N_\phi} + b/N_\phi$. Negative extrapolated values of m^2 suggest a critical or disordered state. In both cases the polynomial, in inverse linear length, fitting form is not justified.

correlation length. For these large values of U_0 , a finite size extrapolation of the square of the local moment (see Fig. 3(b)) is consistent with a finite value (see inset of Fig. 3(b)). In Fig. 3(c) we replot the correlation ratio as a function of U_0 . The data is consistent with a crossing at $U_0 \simeq 3$. Below this value, R does not scale to zero,

as already seen in Fig. 3(a), and hence signals a phase where the correlation length exceeds our system sizes.

Discussion. In Fig. 1 we show possible RG flows in the U_0 versus α plane where α corresponds to the amplitude of a term that breaks down the SO(5) symmetry to SO(3) \times SO(2).

Fig. 1(a) corresponds a scenario where the topological term is irrelevant and the model orders for all values of the stiffness. Taken at face value, our results do not support this point of view. However we cannot exclude the possibility that an ordered phase with small magnetic moment will occur on larger system sizes. In this case, the transition as a function of α from the SO(3) to SO(2) broken symmetries corresponds to a spin-flop transition.

In contrast in Fig. 1(b) we assume that the SO(5) model corresponds to a CFT. In this case, α is a relevant parameter, and the transition from SO(3) to SO(2) broken symmetry phases is continuous with an emergent SO(5) CFT at the critical point. This SO(5) CFT could be a candidate theory for DQCP. Again in light of our data, this scenario seems unlikely since at large values of U_0 our data supports an ordered phase.

In Fig. 1(c) we assume that the observed ordered phase gives way to a critical phase corresponding to an SO(5) CFT. Adding the α axis implies that along the SO(5) line we have a multi-critical point as well as a critical one. Our data actually favors this scenario: below $U_0 = U_0^c \simeq 3$ the correlation ratio does not seem to scale to zero, and is hence consistent with a critical phase. If such is the case, the nature of the transition between SO(3) and SO(2) broken symmetry states, with emergent SO(5) symmetry, depends upon the value of U_0 and is either continuous or first order. There are a number of models that show a transition from SO(2) (VBS/SSC) to SO(3) (AFM/QSH) broken symmetry phases and that favor continuous or weakly first order quantum phase transitions. For instance, 3D loop models¹⁶ ($\eta_{\text{Neel}} = 0.259(6)$, $\eta_{\text{VBS}} = 0.25(3)$), the J-Q model,^{9,26} as well as transitions between quantum spin Hall insulators and s -wave superconductors, ($\eta_{\text{QSH}} = 0.21(5)$, $\eta_{\text{SSC}} = 0.22(6)$)¹⁰ all seem to show similar exponents and are believed to belong to the class of DQCP with emergent spinons coupled to a non-compact U(1) gauge field. Compelling evidence of emergent SO(5) symmetry has been put forward for the loop model.¹⁵ However, the value of the anomalous dimension lies at odds with conformal bootstrap bounds, $\eta > 0.52$,²⁷ for emergent SO(5) symmetry. Systematic drift in the exponents has been observed in.¹⁶ Within the present context one can understand the above in terms fix-point collision put forward in.^{28–31} Consider a third axis – the dimension – and assume that the sketch of Fig. 1(c) is realized *close* to the physical dimension $d = 2$ but that before approaching $d = 2$ the multi-critical and critical points collide and develop a complex component. In this case we are back to the spin-flop transition of Fig. 1(a) but with the important insight that the RG flow

becomes arbitrarily slow due to proximity of a fix-point collision. The shaded region in Fig. 1(a) schematically depicts the region where the RG flow becomes very slow.

Proximity to a critical point motivates fitting the QMC data to the form: $m = m_0 + aN_\phi^{-\frac{\eta+z}{4}}$. In the region where our correlation length exceeds the size of our system we obtain a good fit with robust anomalous dimension $\eta = 0.28(2)$ under the assumption of $z = 1$ (see the SM). The agreement with the aforementioned QMC results is remarkable. We note that this exponent is much larger than the one of the 3D classical O(5) critical point, with $\eta = 0.036(6)$.³² We conclude this section by noting that Ref.³³ introduces a fermion model showing a DQCP with emergent SO(5) symmetry and that has exponents that comply with the bootstrap bounds. This model could be a realization of the SO(5) CFT conjectured in Fig. 1(c).

Fig. 1(d) describes the possibility of an order-disorder transition along the SO(5) line. Note however that on the accessible system sizes, we cannot resolve the length scale associated with the disordered state. This scenario excludes a DQCP with emergent SO(5) symmetry, and the transition from the disordered to ordered phases involve SO(3) or SO(2) critical points. As shown in Fig. 2 the insulating phase has vanishing charge susceptibility. The existence and nature of an SO(5) symmetric disordered phase is intriguing. Starting from Dirac fermions any band insulating state necessarily involves SO(5) symmetry breaking. Hence in the conjectured phase diagram of Fig. 1(d) the disordered phase is not adiabatically connected to a band insulator. In fact, if the disordered phase preserves the particle-hole symmetry, the arguments of Ref.²⁸ rule out *any* gapped phase (even a topological one), because the particle-hole symmetry forbids the SO(5) Hall-conductance argued to be necessary in any such insulator.

Conclusions – Our data on systems up to $N_\phi = 100$ show that the SO(5) non-linear sigma model exhibits an ordered phase in the limit of large stiffness. Remarkably (and within the accessible parameter range where negative sign free AFQMC simulations can be carried out), we observe another regime characterized by a correlation length that exceeds our system size. Given the aforementioned body of work on DQC and insights from the conformal bootstrap approach, our results find a natural interpretation by assuming that the model lies close to a fix-point with small complex component^{28–30} such that the RG flow becomes very slow and shows pseudo-critical behavior. Clearly larger system sizes are desirable so as to confirm this point of view. Although very appealing, as implemented the Landau level projection approach comes with a computational effort that scales as $N_\phi^5 \beta$ as opposed to $N_\phi^3 \beta$ for the generic Hubbard model. Further improvements to the code will have to be implemented so as to reach bigger flux values. The method can also be applied to the O(4) model with θ -term at $\theta = \pi$

by setting one mass term to zero. This will have impact on our understanding of easy plane de-confined quantum critical points with emergent $O(4)$ symmetry.

We would like to thank A. Nahum, W. Guo, T. Senthil and C. Wang for discussions, as well as Matteo Ippoliti with whom we have carried out previous work on this subject. The authors gratefully acknowledge the Gauss Centre for Supercomputing e.V. (www.gauss-centre.eu) for funding this project by providing computing time on the GCS Supercomputer SUPERMUC-NG at Leibniz Supercomputing Centre (www.lrz.de). FFA thanks funding from the Deutsche Forschungsgemeinschaft under the grant number AS 120/15-1 as well as through the Würzburg-Dresden Cluster of Excellence on Complexity and Topology in Quantum Matter - ct.qmat (EXC 2147, project-id 39085490). ZW thanks financial support from the DFG funded SFB 1170 on Topological and Correlated Electronics at Surfaces and Interfaces. MZ was supported by the DOE, office of Basic Energy Sciences under contract no. DEAC02-05-CH11231. RM was supported by the National Science Foundation under grant No. NSF-1848336.

-
- [1] F. F. Assaad and I. F. Herbut, Phys. Rev. X **3**, 031010 (2013).
 - [2] F. Parisen Toldin, M. Hohenadler, F. F. Assaad, and I. F. Herbut, Phys. Rev. B **91**, 165108 (2015).
 - [3] Y. Otsuka, S. Yunoki, and S. Sorella, Phys. Rev. X **6**, 011029 (2016).
 - [4] D. J. Gross and A. Neveu, Phys. Rev. D **10**, 3235 (1974).
 - [5] I. F. Herbut, Phys. Rev. Lett. **97**, 146401 (2006).
 - [6] S. Chandrasekharan and A. Li, Phys. Rev. D **88**, 021701 (2013).
 - [7] T. Senthil, A. Vishwanath, L. Balents, S. Sachdev, and M. P. A. Fisher, Science **303**, 1490 (2004).
 - [8] T. Senthil, L. Balents, S. Sachdev, A. Vishwanath, and M. P. A. Fisher, Phys. Rev. B **70**, 144407 (2004).
 - [9] A. W. Sandvik, Phys. Rev. Lett. **98**, 227202 (2007).
 - [10] Y. Liu, Z. Wang, T. Sato, M. Hohenadler, C. Wang, W. Guo, and F. F. Assaad, Nature Communications **10**, 2658 (2019).
 - [11] S. Ryu, C. Mudry, C.-Y. Hou, and C. Chamon, Phys. Rev. B **80**, 205319 (2009).
 - [12] A. Abanov and P. Wiegmann, Nuclear Physics B **570**, 685 (2000).
 - [13] A. Tanaka and X. Hu, Phys. Rev. Lett. **95**, 036402 (2005).
 - [14] T. Senthil and M. P. A. Fisher, Phys. Rev. B **74**, 064405 (2006).
 - [15] A. Nahum, P. Serna, J. T. Chalker, M. Ortuño, and A. M. Somoza, Phys. Rev. Lett. **115**, 267203 (2015).
 - [16] A. Nahum, J. T. Chalker, P. Serna, M. Ortuño, and A. M. Somoza, Phys. Rev. X **5**, 041048 (2015).
 - [17] F. D. M. Haldane, Phys. Rev. B **25**, 4925 (1982).
 - [18] C. Mudry, A. Furusaki, T. Morimoto, and T. Hikihara, Phys. Rev. B **99**, 205153 (2019).
 - [19] M. Weber, F. Parisen Toldin, and M. Hohenadler, “Competing Orders and Unconventional Criticality in the Su-Schrieffer-Heeger Model,” (2019), arXiv:1905.05218 [cond-mat.str-el].
 - [20] M. Ippoliti, R. S. K. Mong, F. F. Assaad, and M. P. Zaletel, Phys. Rev. B **98**, 235108 (2018).
 - [21] J. Lee and S. Sachdev, Phys. Rev. Lett. **114**, 226801 (2015).
 - [22] R. Blankenbecler, D. J. Scalapino, and R. L. Sugar, Phys. Rev. D **24**, 2278 (1981).
 - [23] S. White, D. Scalapino, R. Sugar, E. Loh, J. Gubernatis, and R. Scalettar, Phys. Rev. B **40**, 506 (1989).
 - [24] F. Assaad and H. Evertz, in *Computational Many-Particle Physics*, Lecture Notes in Physics, Vol. 739, edited by H. Fehske, R. Schneider, and A. Weiße (Springer, Berlin Heidelberg, 2008) pp. 277–356.
 - [25] M. Bercx, F. Goth, J. S. Hofmann, and F. F. Assaad, SciPost Phys. **3**, 013 (2017).
 - [26] H. Shao, W. Guo, and A. W. Sandvik, Science **352**, 213 (2016).
 - [27] D. Poland, S. Rychkov, and A. Vichi, Rev. Mod. Phys. **91**, 015002 (2019).
 - [28] C. Wang, A. Nahum, M. A. Metlitski, C. Xu, and T. Senthil, Phys. Rev. X **7**, 031051 (2017).
 - [29] A. Nahum, “Note on Wess-Zumino-Witten models and quasiuniversality in 2+1 dimensions,” (2019), arXiv:1912.13468 [cond-mat.str-el].
 - [30] R. Ma and C. Wang, “A theory of deconfined pseudocriticality,” (2019), arXiv:1912.12315 [cond-mat.str-el].
 - [31] I. F. Herbut and L. Janssen, Phys. Rev. Lett. **113**, 106401 (2014).
 - [32] Q. Liu, Y. Deng, T. M. Garoni, and H. W. Blöte, Nuclear Physics B **859**, 107 (2012).
 - [33] Z.-X. Li, S.-K. Jian, and H. Yao, “Deconfined quantum criticality and emergent $so(5)$ symmetry in fermionic systems,” (2019), arXiv:1904.10975 [cond-mat.str-el].
 - [34] Z.-X. Li, Y.-F. Jiang, and H. Yao, Phys. Rev. Lett. **117**, 267002 (2016).

SUPPLEMENTAL MATERIAL

Landau Level projection

We consider electrons confined to the two-dimensional x-y plane and in a transverse magnetic field:

$$\hat{H}_0 = \frac{1}{2m} \left(\hat{\mathbf{P}} - e\mathbf{A}(\mathbf{r}) \right)^2. \quad (9)$$

In the Landau gauge, $\mathbf{A}(\mathbf{r}) = B(0, x, 0)$ ($\mathbf{r} = (x, y, z)$), translations along the y direction leave the Hamiltonian invariant such that the momentum in this axis, p_y , is a good quantum number. On a torus of size $L_x \times L_y$ the wave function of the first Landau level reads:

$$\phi_{p_y}(\mathbf{r}) = \frac{1}{\sqrt{L_y}} \frac{1}{\sqrt{l_B \sqrt{\pi}}} e^{-(x/l_B - \text{sign}(B)p_y l_B)^2/2} e^{ip_y y}. \quad (10)$$

Here the magnetic length scale is defined as $l_B^2 = \frac{\phi_0}{2\pi|B|}$, with $\phi_0 = \frac{h}{e}$, and the number of magnetic fluxes piercing the system, $N_\phi = \frac{|B|V}{\phi_0}$, is an integer so as to guarantee uniqueness of the wave function. Finally the momentum in the y-direction is given $p_y = \frac{2\pi n}{L_y}$ with $n \in 1, \dots, N_\phi$. From here onwards we will consider

The orbital wave function of the first Landau level of free electrons in a magnetic field and that of the zero energy Landau level (ZLL) in graphene are identical. In graphene, however, there is an SU(4) symmetry such the electron carries an additional flavor index, $a \in 1, \dots, 4$. Let $\hat{c}_{p_y, a}$ destroy an electron in the ZLL with flavor index a and momentum p_y . These operators satisfy canonical fermion commutation rules:

$$\left\{ \hat{c}_{p_y, a}^\dagger, \hat{c}_{p'_y, a'} \right\} = \delta_{a, a'} \delta_{p_y, p'_y}, \quad \left\{ \hat{c}_{p_y, a}, \hat{c}_{p'_y, a'} \right\} = 0. \quad (11)$$

Our Hamiltonian is defined in terms of projected field operators.

$$\hat{\psi}_a(\mathbf{r}) = \sum_{p_y=1}^{N_\phi} \phi_{p_y}(\mathbf{r}) \hat{c}_{a, p_y}. \quad (12)$$

Since the ZLL does not span the Hilbert space the projected field operators do not satisfy the fermion canonical commutation rules, and before formulating the AFQMC we have to express everything in terms of the canonical operators \hat{c}_{a, p_y} . Defining the Fourier transform of the four component spinor:

$$\hat{\psi}_a^\dagger = \frac{1}{\sqrt{V}} \int_V d^2\mathbf{r} e^{i\mathbf{p} \cdot \mathbf{r}} \hat{\psi}_a^\dagger(\mathbf{r}) \quad (13)$$

we obtain

$$\begin{aligned} \hat{H} &= \sum_{i=0}^5 \int_V d^2\mathbf{r} \frac{U_i}{2} [\hat{\psi}_a^\dagger(\mathbf{r}) O_{ab}^i \hat{\psi}_b(\mathbf{r}) - C(\mathbf{r}) \delta_{i,0}]^2 \\ &= \sum_{i=0}^5 \frac{U_i}{2} \sum_{\mathbf{q}} \sum_{\mathbf{q}'} \int_V d^2\mathbf{r} \left(\frac{1}{V} e^{i\mathbf{q} \cdot \mathbf{r}} \hat{N}^i(\mathbf{q}) \right) \left(\frac{1}{V} e^{i\mathbf{q}' \cdot \mathbf{r}} \hat{N}^i(\mathbf{q}') \right) \\ &= \frac{1}{2V} \sum_{i=0}^5 \sum_{\mathbf{q}} \hat{N}^i(\mathbf{q}) U_i \hat{N}^i(-\mathbf{q}) \end{aligned} \quad (14)$$

Here, O^0 , is the unit matrix and $\hat{\psi}_a^\dagger(\mathbf{r}) O^i \hat{\psi}_b(\mathbf{r}) = \frac{1}{V} \sum_{\mathbf{q}} e^{-i\mathbf{q} \cdot \mathbf{r}} \hat{N}^i(\mathbf{q})$ for $i = 1 \dots 5$ and $\hat{\psi}_a^\dagger(\mathbf{r}) \hat{\psi}_b(\mathbf{r}) - C(\mathbf{r}) = \frac{1}{V} \sum_{\mathbf{q}} e^{-i\mathbf{q} \cdot \mathbf{r}} \hat{N}^0(\mathbf{q})$

Neglecting the constant background term at $i = 0$, the *density* operators $\hat{N}^i(\mathbf{q})$, can be expressed in terms of the canonical operators $\hat{c}_{p_y}^\dagger$:

$$\begin{aligned} \hat{N}^i(\mathbf{q}) &= \sum_{\mathbf{p}} \hat{\psi}_a^\dagger O^i \hat{\psi}_{\mathbf{p}-\mathbf{q}} \\ &= \frac{1}{V} \sum_{\mathbf{p}} \int_V \int_{V'} d^2\mathbf{r} d^2\mathbf{r}' e^{i\mathbf{p} \cdot \mathbf{r}} e^{-i(\mathbf{p}-\mathbf{q}) \cdot \mathbf{r}'} \\ &\quad \sum_{k_1} \hat{c}_{k_1}^\dagger \phi_{k_1}^*(\mathbf{r}) O^i \sum_{k_2} \hat{c}_{k_2} \phi_{k_2}(\mathbf{r}') \\ &= \frac{1}{V} \sum_{\mathbf{p}} \sum_{k_1} \sum_{k_2} \hat{c}_{k_1}^\dagger O^i \hat{c}_{k_2} \int_V \int_{V'} d^2\mathbf{r} d^2\mathbf{r}' \\ &\quad \left(\frac{1}{\sqrt{L_y}} \frac{\pi^{-\frac{1}{4}}}{\sqrt{l_B}} e^{-ik_1 y} e^{-\frac{1}{2}(\frac{x}{l_B} - k_1 l_B)^2} e^{i\mathbf{p} \cdot \mathbf{r}} \right) \\ &\quad \cdot \left(\frac{1}{\sqrt{L_y}} \frac{\pi^{-\frac{1}{4}}}{\sqrt{l_B}} e^{+ik_2 y'} e^{-\frac{1}{2}(\frac{x'}{l_B} - k_2 l_B)^2} e^{i(\mathbf{p}-\mathbf{q}) \cdot \mathbf{r}'} \right) \\ &= \sum_{\mathbf{p}} \frac{2l_B \pi^{1/2}}{L_x} e^{ip_x p_y l_B^2} e^{-l_B^2 p_x^2/2} \\ &\quad e^{i(p_x - q_x)(p_y - q_y)l_B^2} e^{-l_B^2 (p_x - q_x)^2/2} \hat{c}_{p_y}^\dagger O^i \hat{c}_{p_y - q_y} \\ &= \frac{1}{2\sqrt{\pi}} e^{-l_B^2 q^2/4} \sum_{p_y} e^{iq_x p_y l_B^2} \hat{c}_{p_y + \frac{q_y}{2}}^\dagger O^i \hat{c}_{p_y - \frac{q_y}{2}} \end{aligned} \quad (15)$$

In the last step, the sum over p_x is carried out by changing sums to integrals and taking the limit $L_x \rightarrow \infty$. With the substitution $k = p_y + \frac{q_y}{2}$ and

$$\begin{aligned} \hat{n}^i(\mathbf{q}) &= \sum_{k=1}^{N_\phi} \sum_{a,b=1}^4 F(\mathbf{q}) e^{\frac{i}{2}(2k - q_y)l_B^2 q_x} (\hat{c}_{a,k}^\dagger O_{a,b}^i \hat{c}_{b,k - q_y} \\ &\quad - 2\delta_{q_y,0} \delta_{i,0}) \end{aligned} \quad (16)$$

the Hamiltonian reads:

$$\hat{H} = \frac{1}{8\pi V} \sum_{i=0}^5 \sum_{\mathbf{q}} \hat{n}^i(\mathbf{q}) U_i \hat{n}^i(-\mathbf{q}). \quad (17)$$

In the above, $a(b) = 1, 2, 3$ and 4 is the flavor index, and $F(\mathbf{q}) \equiv e^{-\frac{1}{4}(q_x^2 + q_y^2)l_B^2}$. The background term $2\delta_{q_y,0} \delta_{i,0}$

can easily be verified by Fourier transform the real space background $C(\mathbf{r})$ (see main text).

As we will shown in the next subsection, this exponential decaying factor is essential for the QMC simulation since it provides a natural cutoff for the momenta \mathbf{q} . Finally, setting the magnetic unit length to unity such that $\frac{2\pi}{V} = \frac{1}{N_\phi}$ we obtain:

$$\hat{H} = \frac{1}{16\pi^2 N_\phi} \sum_{i=0}^5 \sum_{\mathbf{q}} \hat{n}^i(\mathbf{q}) U_i \hat{n}^i(-\mathbf{q}) \quad (18)$$

Fierz identity and absence of the negative sign problem

To avoid the negative sign problem in the QMC simulations we use the Fierz identity to rewrite Eq. (14) as:

$$H = \frac{1}{2N_\phi} \sum_{i=0}^3 \sum_{\mathbf{q}} \hat{n}_{-\mathbf{q}}^i g^i \hat{n}_{\mathbf{q}}^i \quad (19)$$

Instead of the original density operators in Eq. (16), the $n^i (i = 0, 1, 2, 3)$ operators are based on 4 matrix:

$$\mathbb{I}_4, \tau_x \otimes \mathbb{I}_2, \tau_y \otimes \mathbb{I}_2, \tau_z \otimes \mathbb{I}_2. \quad (20)$$

Eq. (19) is identical to Eq. (14) when $\frac{g^0}{8\pi^2} = U_0 + U$, $\frac{g^1}{8\pi^2} = \frac{g^2}{8\pi^2} = -2U$, and $\frac{g^3}{8\pi^2} = 2U$. Here we consider the SO(5) symmetric point and set $U_i = -U$ for $i \in 1, \dots, 4$. The absence of sign problem holds for the region of $U_0 \geq -U$, follows from the work of Ref.³⁴ and is discussed in detail in reference.²⁰ The above matrix structure also gives an explicit $SU(2)$ symmetry which holds for each Hubbard-Stratonovich field configuration.

Trotter errors

Since $n(\mathbf{q})^\dagger = n(-\mathbf{q})$, the exponential of operators at each time slice is given by:

$$\begin{aligned} & e^{-\frac{\Delta\tau}{2N_\phi} (\hat{n}_{\mathbf{q}}^i g^i \hat{n}_{-\mathbf{q}}^i + \hat{n}_{-\mathbf{q}}^i g^i \hat{n}_{\mathbf{q}}^i)} \\ &= e^{-\frac{\Delta\tau}{4N_\phi} [g^i (\hat{n}_{\mathbf{q}}^i + \hat{n}_{-\mathbf{q}}^i)^2 - g^i (\hat{n}_{\mathbf{q}}^i - \hat{n}_{-\mathbf{q}}^i)^2]} \end{aligned} \quad (21)$$

To ensure hermiticity, we use a symmetric Trotter decomposition:

$$Z = \text{Tr} \left[\prod_{m=1}^N e^{-\frac{\Delta\tau}{2} \hat{H}_m} \prod_{n=N}^1 e^{-\frac{\Delta\tau}{2} \hat{H}_n} \right]^{L_\tau} \quad (22)$$

where \hat{H}_m corresponds to the $N = 2 \times 4 \times N_q$ operators $\pm \frac{g^i}{4N_\phi} (\hat{n}_{\mathbf{q}}^i \pm \hat{n}_{-\mathbf{q}}^i)^2$. N_q is the number of momentum points used for the simulation. As we will see below N_q scales as N_ϕ .

For two operators \hat{H}_1 and \hat{H}_2 the leading order error produced in the symmetric Trotter decomposition reads:

$$\begin{aligned} & e^{-\frac{\Delta\tau}{2} \hat{H}_1} e^{-\Delta\tau \hat{H}_2} e^{-\frac{\Delta\tau}{2} \hat{H}_1} \\ &= e^{-\Delta\tau (\hat{H}_1 + \hat{H}_2) + \frac{\Delta\tau^3}{12} [2\hat{H}_1 + \hat{H}_2, [\hat{H}_1, \hat{H}_2]]} + \mathcal{O}(\Delta\tau^4) \end{aligned} \quad (23)$$

Iterating the above formula gives:

$$\prod_{m=1}^N e^{-\frac{\Delta\tau}{2} \hat{H}_m} \prod_{n=N}^1 e^{-\frac{\Delta\tau}{2} \hat{H}_n} = e^{-\Delta\tau ((\sum_{m=1}^N \hat{H}_m) + \hat{\lambda})} + \mathcal{O}(\Delta\tau^4) \quad (24)$$

where

$$\begin{aligned} \hat{\lambda} \equiv & -\frac{\Delta\tau^2}{12} \left(\sum_{m=1}^{N-1} \sum_{m'=m+1}^N [2\hat{H}_m + \hat{H}_{m'}, [\hat{H}_m, \hat{H}_{m'}]] \right. \\ & \left. + \sum_{m=1}^{N-1} \sum_{m'=m+1}^N \sum_{m''=m+1}^N [\hat{H}_{m'}, [\hat{H}_m, \hat{H}_{m''}]] (1 - \delta_{m', m''}) \right) \end{aligned} \quad (25)$$

and $\delta_{m', m''}$ the Kronecker delta. Using time dependent perturbation theory, we then obtain:

$$\begin{aligned} & \left(\prod_{m=1}^N e^{-\frac{\Delta\tau}{2} \hat{H}_m} \prod_{n=N}^1 e^{-\frac{\Delta\tau}{2} \hat{H}_n} \right)^{L_\tau} \\ &= e^{-\beta \hat{H}} - e^{-\beta \hat{H}} \int_0^\beta d\tau e^{\tau \hat{H}} \hat{\lambda} e^{-\tau \hat{H}} + \mathcal{O}(\Delta\tau^3) \end{aligned} \quad (26)$$

with $L_\tau = \frac{\beta}{\Delta\tau}$ the number of time slices. $\hat{\lambda}$ is measure of the leading order error on the free energy density:

$$\begin{aligned} f_{QMC} &\equiv -\frac{1}{\beta V} \ln \text{Tr} \left(\prod_{m=1}^N e^{-\frac{\Delta\tau}{2} \hat{H}_m} \prod_{n=N}^1 e^{-\frac{\Delta\tau}{2} \hat{H}_n} \right)^{L_\tau} \\ &= f + \frac{1}{\beta V} \int_0^\beta d\tau \langle e^{\tau \hat{H}} \hat{\lambda} e^{-\tau \hat{H}} \rangle + \mathcal{O}(\Delta\tau^3) \\ &= f + \frac{1}{V} \langle \hat{\lambda} \rangle + \mathcal{O}(\Delta\tau^3) \\ &= f + \frac{1}{2\pi N_\phi} \langle \hat{\lambda} \rangle + \mathcal{O}(\Delta\tau^3) \end{aligned} \quad (27)$$

In the above we have set $l_B = 1$ so as to replace V by N_ϕ , and $f = -\frac{1}{\beta V} \ln \text{Tr} e^{-\beta \hat{H}}$. Since the interacting operators for different masses i do not commute with each other, the Trotter decomposition breaks the SO(5) symmetry of Hamiltonian (a $SU(2)$ symmetry is left due to the Fierz identity in Eq. (19)).

To evaluate the expectation value of $\hat{\lambda}$, we first evaluate

the commutator of two density operators:

$$\begin{aligned}
& [\hat{n}^i(\mathbf{q}_1), \hat{n}^j(\mathbf{q}_2)] \\
&= F(\mathbf{q}_1)F(\mathbf{q}_2) \sum_k \hat{\mathbf{c}}_k^\dagger \{e^{\frac{i}{2}(2k-(q_{1y}+q_{2y}))l_B^2(q_{1x}+q_{2x})} \\
&\quad (2\cos(\theta_{\mathbf{q}_1, \mathbf{q}_2})[O_i, O_j] + 2i\sin(\theta_{\mathbf{q}_1, \mathbf{q}_2})\{O_i, O_j\})\} \hat{\mathbf{c}}_{k-(q_{1y}+q_{2y})} \\
&= \frac{F(\mathbf{q}_1)F(\mathbf{q}_2)}{F(\mathbf{q}_1 + \mathbf{q}_2)} \{n^{[O_i, O_j]}(\mathbf{q}_1 + \mathbf{q}_2) 2\cos(\theta_{\mathbf{q}_1, \mathbf{q}_2}) \\
&\quad + n^{\{O_i, O_j\}}(\mathbf{q}_1 + \mathbf{q}_2) 2i\sin(\theta_{\mathbf{q}_1, \mathbf{q}_2})\}
\end{aligned} \quad (28)$$

where $\theta_{\mathbf{q}_1, \mathbf{q}_2} = \frac{l_B^2}{2}(q_{1y}q_{2x} - q_{1x}q_{2y})$. Since the density operators do not commute we can estimate the magnitude of the Trotter error as follows. Let $\|\hat{A}\| \equiv \max_{|\Psi\rangle, \|\Psi\|=1} \|\hat{A}|\Psi\rangle\|$. Since the Hamiltonian $\sum_m H_m$ is an extensive quantity, $\|\sum_m H_m\| \propto N_\Phi$. Here m runs over a set of order N_Φ momenta, hence implies that typically, $H_m \propto N_\Phi^0$. Using this to estimate the systematic error, yields the result:

$$f_{QMC} = f + \mathcal{O}(\Delta\tau^2 N_\Phi^2). \quad (29)$$

Hence, to keep the Trotter error under control we have to scale $\Delta\tau$ as $1/N_\Phi$.

The Trotter error in our model has a different scaling behavior, than for models with only local interaction such as the Hubbard model. For local interactions $\|\lambda\|$ scales as N_Φ , such that the systematic error on the free energy density is size independent.

An improved estimator is introduced, based on the SO(5) invariant structure factor:

$$S(\mathbf{q}) = \frac{1}{N_\Phi} \sum_{i=1}^5 \langle \hat{n}_{\mathbf{q}}^i \hat{n}_{-\mathbf{q}}^i \rangle. \quad (30)$$

The magnetization and correlation ratio used for the scaling analysis in the main part of the paper is based on the above structure factor.

Fig. 4 shows a numerical comparison of the correlation ratio for multiple system sizes. In Fig. 4 (a) we consider a constant $\Delta\tau$ while in Fig. 4 (b) we scale $\Delta\tau$ with the volume: $\Delta\tau = 25.6\pi^2/N_\Phi$. As mentioned previously, our Trotter decomposition breaks the SO(5) symmetry such that a convenient measure of the finite time step systematic error is the discrepancy between the Néel and VBS order parameters. At constant $\Delta\tau = 3.2\pi^2$ the correlation ratio defined from the Néel, VBS and SO(5) order parameters progressively differ as a function of system size. On the other hand, for simulations where we keep $\Delta\tau N_\Phi$ constant, see Fig. 4 (b), no SO(5) symmetry breaking up to $N_\Phi = 32$ is apparent. In all our simulations we have kept $\Delta\tau N_\Phi$ constant.

Cutoff

The effective interacting strength in Eq. (19) is controlled by a momentum dependent function $F(\mathbf{q})$ in

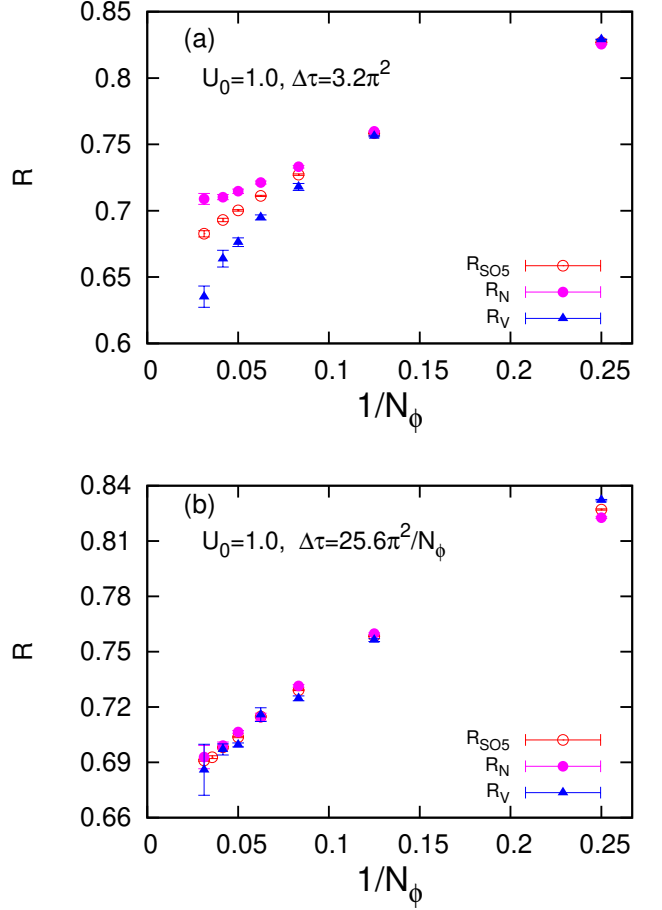


FIG. 4. Correlation ratio R of Neel, VBS order and the improved estimator for a fix $\Delta\tau$ as $3.2\pi^2$ (a), and for a linear scaling of $\Delta\tau = 25.6\pi^2/N_\Phi$ (b). The simulation is based on $U_0 = 1.0$, of system sizes $N_\Phi = 4, 8, 12, 16, \dots, 32$, with $\beta = 1$.

Eq. (16):

$$F(\mathbf{q}) = e^{-\frac{1}{4}(q_x^2 + q_y^2)l_B^2} \quad (31)$$

The exponential decay of the interacting strength gives a natural cutoff in the momentum space. In particular, we can consider momenta satisfying $F(\mathbf{q}) > F_{min}$. As shown in Fig. 5, for $N_\Phi = 4, 8$ and 12 at $U_0 = U = 1$, the cutoff dependence of the correlation ratio is negligible up to $F_{min} = 0.01$. In our calculations, we have chosen $F_{min} = 0.01$. Setting $l_B = 1$ implies that the number of \mathbf{q} -vectors we consider for a given cutoff scales as N_Φ .

Comparison to exact diagonalisation

A benchmark calculation of QMC with the exact diagonalization(ED) is performed, based on comparing exact ground state of a half filled system, to a finite temperature AFQMC simulation at low enough temperature ($\beta =$

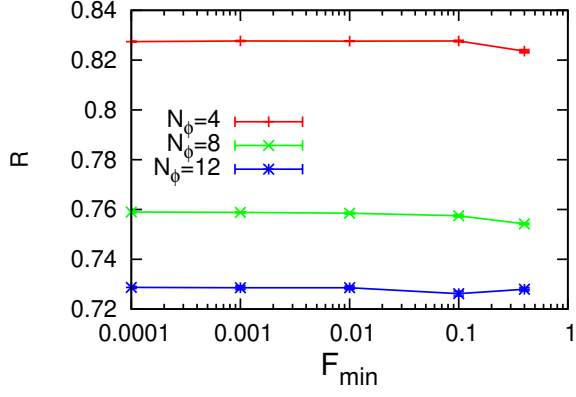


FIG. 5. Correlation ratio as a function of F_{min} for $N_\phi = 4, 8$ and 12 , at $U_0 = U = 1, \beta = 160\pi^2, \Delta\tau = 3.2\pi^2$.

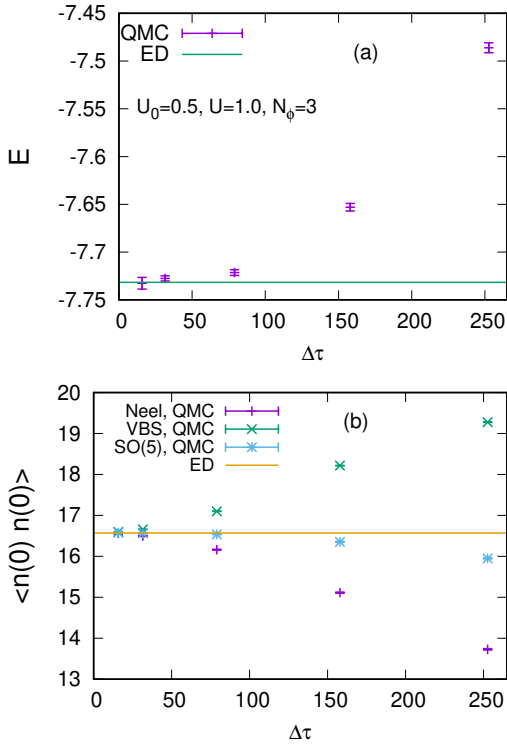


FIG. 6. Ground state energy (a) and magnetic order parameter (b) based on AFQMC as a function of $\Delta\tau$, as well as ED. The calculation is performed at $U_0 = 0.5, U = 1.0$ for $N_\phi = 3$.

$320\pi^2$). As an example we consider $U_0 = 0.5, U = 1.0$ at $N_\phi = 3$. In Fig. 6, we see that the two methods show consistent results for the ground state energy and the SO(5) invariant correlation function at zero momentum in the limit of small $\Delta\tau$. Both the Neel(VBS) correlation function based on the average value of density operators of only the $i = 1, 2, 3$ (4, 5) term in Eq. (30) are equally shown in Fig. 6(b).

U_0	$\langle m \rangle_0$	η	χ^2/DOF
-1.0	0.03(1)	0.33(2)	1.51
-0.5	0.01(1)	0.28(2)	1.32
0.0	0.03(1)	0.29(2)	1.78
0.25	0.028(7)	0.27(1)	0.92
0.5	0.04(1)	0.28(2)	0.25
1.0	0.05(1)	0.28(2)	1.17
2.0	0.064(7)	0.26(2)	0.98
4.0	0.11(1)	0.26(2)	1.75
8.0	0.27(1)	0.38(2)	1.11

TABLE I. Collective fit using Eq. (32).

Fitting of the magnetization: proximity to fix-point collision

Another assumption is that, the ground state in the cases of $U_0 > 0$ is always in a $O(5)$ symmetry breaking phase, with a small magnetization. Here we show the fit details based on:

$$m = m_0 + aN_\phi^{-\frac{\eta+z}{4}} \quad (32)$$

As we can see from Table I, the χ^2/DOF of fit are acceptable, when all the system sizes are included. The η exponent is robust as function of U_0 , except the point of $U_0 = 8$. On the other hand, the extrapolated magnetization become nonzero within when $U_0 \geq 0.25$.